Classification of spontaneous oscillations at the onset of avalanche breakdown in *p*-type germanium

U. Rau, W. Clauss, A. Kittel, M. Lehr, M. Bayerbach, J. Parisi,
J. Peinke, and R. P. Huebener
Physikalisches Institut, Lehrstuhl Experimentalphysik II, Universität Tübingen, Auf der Morgenstelle 14, D-7400 Tübingen, Federal Republic of Germany
(Received 28 December 1989; revised manuscript received 2 July 1990)

We present a detailed study on the oscillatory behavior of *p*-type germanium at the onset of avalanche breakdown at low temperatures. Measuring the frequency and amplitude of these oscillations as a function of different control parameters, such as average current, perpendicular magnetic field, and outer circuit conditions, we can clearly distinguish two different types of oscillations. For one, we found an oscillatory mechanism that depends on the outer electrical circuit. It describes the behavior in detail and also clarifies the connection between the dynamical behavior and the actual appearance of the current-voltage characteristic. Whereas this first type is the result of a global mechanism involving sample voltage and sample resistance, the second type results from a local oscillatory mechanism. Therefore, the more complicated dynamical structure can be understood as a result of the coupling between different localized oscillatory modes.

I. INTRODUCTION

It is a well-known fact that a variety of electrical systems displays spontaneous formation of spatial and temporal structures as a consequence of transport instabilities connected to a region of negative differential (ND) resistance in their current-voltage (*I-V*) characteristics. Commonly, these instabilities can be classified as either *N*-shaped or *S*-shaped ND resistive systems, and it is well understood that a microscopic ND resistivity induces inhomogeneous spatial structures, such as high-field domains (in the case of *N* shape) or high-current filaments (for the *S* shape).[1] As a consequence, the form of the *I-V* characteristic observed on the macroscopic level not only depends on the underlying microscopic *N* or *S*, but is also the result of the different spatial mechanisms; for example, the gradual growth or shrinking of structures[2] or the switching between different conducting states.[3] Beyond that, one of the main objectives of the present paper is to show that the actual appearance of the *I-V* characteristic in some regions is a consequence of an underlying dynamical structure. So far, one can conclude from the observation of the macroscopic ND resistance behavior the *existence* of a corresponding microscopic ND resistivity (yet not in the inverse direction[2]), but not in its *details*. In the following, we concentrate on the case of *S*-shaped ND resistance, but we emphasize that some general features of our results might also be applicable to *N*-shaped ND resistive systems.

The behavior of an *S*-shaped electrical system can be understood as a nonequilibrium phase transition of a low conducting state to a high conducting state.[2,4] The resulting formation of current filaments has been observed recently in many experimental systems, such as bulk semiconductors,[5] semiconductor devices,[6] and gaseous plasma discharges,[7] but most of these systems also display the formation of spontaneous oscillations in the same parameter regime.[8–13]

The occurrence of spontaneous oscillations in electrical circuits containing an element displaying *S*-shaped (current controlled) ND resistance has been a well-known fact for many decades.[14] From the standpoint of electrical engineering, this is due to the fact that it is not possible to apply current control to any device in arbitrarily short times due to the capacitance associated with every electrical circuitry. Moreover, it is customary to construct oscillators using devices displaying ND resistance which are embedded in an appropriate electrical environment. However, the points in this paper are the following: Generally, a system displaying *S*-shaped ND resistance and driven into the range of bistability has two possibilities to realize a certain current fixed by the outer circuitry (high load resistor), namely, either in the temporal average (spontaneous oscillations) or in the spatial average (current filaments). So far, the formation of spatial and temporal structures has to be understood as competing effects, and a complete understanding of these systems has to cover spatial and temporal structures as well as the close relationship between them. The present paper is concerned with the description of different oscillatory *modes*, their spatial character, and the question whether their behavior depends on the outer circuitry or not.

Our experiments deal with the physical mechanism of avalanche breakdown in *p*-type germanium at low temperatures where the transition is due to the autocatalytic character of the underlying impact ionization process.[4,15] This exemplary system shows the features of spontaneous formation of current filaments and oscillations, as mentioned above.[5,8] The oscillatory behavior was systematically examined under variation of different physical parameters, such as perpendicular magnetic field, temperature of the Ge crystal, contact distance, total current, and the bias conditions of the sample. From the results obtained, we can clearly distinguish between two different types of oscillatory behavior. These oscillations can be

 ©1991 The American Physical Society

understood in close connection with the formation of current filaments and the actual appearance of the ND resistance in the I-V characteristic. Further, we present a simple model for one type of oscillatory behavior which is in good agreement with the experimental observations.

This paper is organized as follows. First, we briefly explain the physics of avalanche breakdown in extrinsic germanium at low temperatures and our experimental procedures. Subsequently, we report a first group of experimental results, demonstrating the main features of the two types of oscillations. One type of these oscillations can be described quantitatively by a simple switching model. Finally, we end up with a second group of experiments and a discussion of the dynamical behavior with respect to the formation of spatial structures.

II. PHYSICS OF AVALANCHE BREAKDOWN AND THE EXPERIMENTAL SETUP

Our experiments were performed on single-crystalline p-type germanium (acceptor concentration about 3×10^{14} cm^{-3}, acceptor level about 12 meV). An electrical field could be applied by ohmic contacts (B^+ ion implanted or Al alloyed) on the surface of the sample. At low temperatures, most charge carriers are frozen out at the impurities and the sample nearly acts as an electrical insulator. The few remaining carriers are heated up more and more to energies which at a typical electrical field strength of about 4–4.5 V/cm become sufficient to ionize the neutral impurities, and the impact ionization process arises in the bulk of the semiconductor. Here the concentration of free charge carriers (holes) increases from about $n<10^7 cm^{-3}$ to $n>10^{13}$ cm^{-3}.[15] Note that it is just at the onset of avalanche breakdown where we find the typical nonlinear features of this p-type Ge system, i.e., the formation of current filaments, spontaneous oscillations, and ND resistance. The temperature range yielding the above physics is given by $T<6.2$ K.[16]

Most of the results presented in this paper are related to a p-type Ge crystal having dimensions of about $9.00\times2.88\times0.26$ mm^3 and the crystallographic growth axis oriented in the [111] direction. Properly arranged ohmic Al contacts were evaporated and alloyed on one of the largest surfaces of the sample, with a contact distance of 3.44 mm. We emphasize that all features discussed in the following could be found in several p-type Ge samples, independent of their contact distance (down to 10 μm), contact width, the kind of contacts (ion implanted or Al alloyed), and the orientation of the crystal. Similar results could also be obtained in n-type GaAs (Refs. 13 and 17) and n-type InP.[18] During our experiments, the sample was always in direct contact with the liquid-helium bath and shielded against external irradiation. The bath temperature was 4.18 K. A perpendicular magnetic field up to 100 mT could also be applied. The sample was connected to a series combination of a voltage source V_0 and a load resistor R_L (see Fig. 1). The dc and ac currents were measured via the voltage drop at the load resistor. To obtain the I-V characteristic, the sample voltage was measured along the sample with a high-impedance voltmeter. As a further element of the outer circuit, we have to take into account a capacitance connected in parallel to the sample which is given by the instruments, the cable circuitry, and the sample itself.

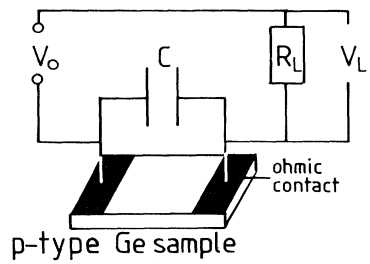

FIG. 1. Experimental setup (schematic) of a p-type germanium experiment. A bias voltage V_0 is applied to the series combination of the sample and a load resistor R_L. Further, we have taken into account the capacitance given by the cables, the instruments, and the sample. Thus the voltage drop V_L at the load resistor is proportional to the current passing through the sample and charging the capacitance C.

III. EXPERIMENTAL RESULTS I—TWO TYPES OF OSCILLATORY BEHAVIOR

The measurement of an ND resistive I-V characteristic strongly depends on the chosen load resistor R_L as an element of the outer electrical circuit. In our experiments, we used load resistors in the range 10 k$\Omega\le R_L\le1$ MΩ, successively approaching the case of current control. There we observed almost nonhysteretic S-shaped dc characteristics. In Fig. 2, we display an I-V characteristic measured with $R_L=100$ kΩ.

Let us now look at the dynamical behavior of the system. We observed spontaneous oscillations of the current almost in the whole range of ND resistance at the onset of avalanche breakdown (dc currents between some 100 nA and 1 mA). In Figs. 3(a)–3(d), we display typical examples of these spontaneous oscillations. The different times traces refer to the points a–d marked in the dc I-V characteristic of Fig. 2. The first occurrence of spontane-

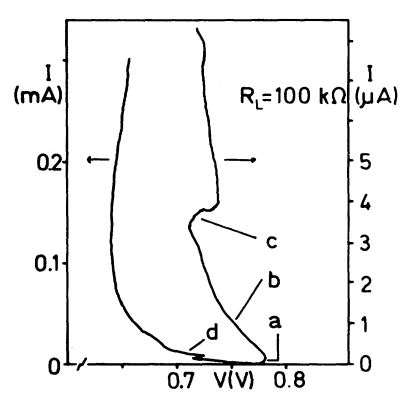

FIG. 2. Typical I-V characteristic of a p-type Ge sample. Current controlled measurement ($R_L=100$ kΩ) in two resolutions. The I-V parameter values of the observed spontaneous oscillations as presented in Figs. 3(a)–3(d) are indicated. Parameters for the measurement are $T=4.18$ K and $B=0$ mT.

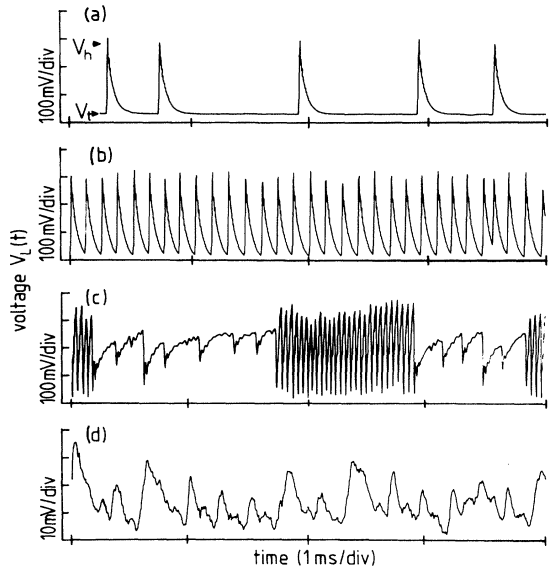

FIG. 3. Spontaneous oscillations observed at different dc current values (as indicated in Fig. 2) and the constant parameters $T=4.18$ K, $B=0$ mT, and $R_L=100$ kΩ. Note that the time signal (d) is stretched by a factor of 10 compared to the other traces.

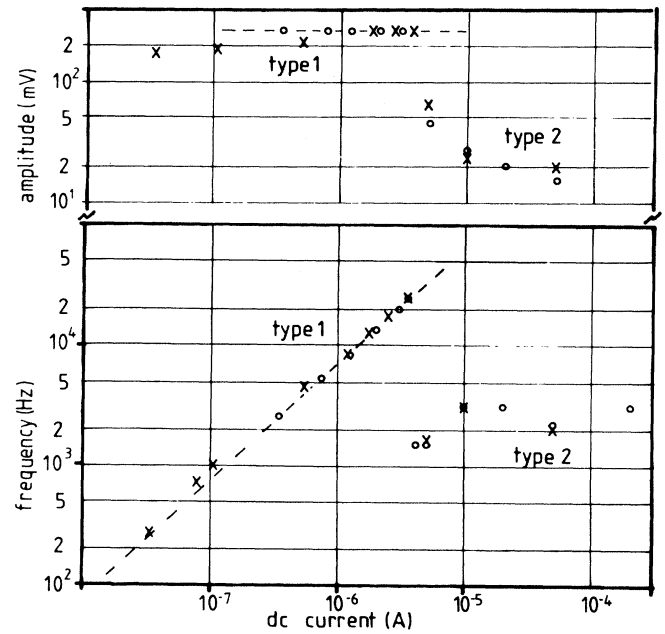

FIG. 4. Log-log plot of the observed (mean peak-to-peak) amplitudes (upper part) and frequencies (lower part) of the spontaneous oscillations vs the mean dc current. Two different load resistors were applied: 100 kΩ (circles) and 1 MΩ (crosses). The amplitudes are those of the ac voltage at the load resistor. Thus, the ac current can be obtained from the voltage divided by the applied load resistor R_L.

ous oscillations is connected to the onset of breakdown, but it still appears in the positive differential resistance region of the characteristic [see Fig. 3(a)]. Here the oscillation seems to be stochastic, but it becomes more and more regular without changing its shape or amplitude with increasing bias voltage [Fig. 3(b)]. At a sample voltage of 0.781 V, where the *I-V* characteristic enters its ND resistive branch, this oscillation becomes periodic. On increasing the bias voltage further, the frequency of this oscillation increases up to 30 kHz, corresponding to a dc current of about 3 μA. There, a drastic change in the dynamical behavior connected to a distinct step in the *I-V* characteristic (see Fig. 2) occurs. The temporal signal at this point [Fig. 3(c)] displays an intermittent switching between the oscillation form described above and another oscillation which is characterized by a lower amplitude and a lower frequency in the range of 2 kHz. On increasing the bias voltage further, only this new oscillation survives [Fig. 3(d)].

To summarize the oscillatory behavior, we have plotted the frequency and the mean peak-to-peak amplitude of the spontaneous oscillations vs the mean current transported along the sample in Fig. 4. Here in the range of 50 nA to 3 μA, we find a strict proportionality between the frequency of the spontaneous oscillations and the dc current, whereas the amplitude (except for some values at currents lower than 200 nA) remains nearly constant at a value of about 250 mV, obtained as the dynamical voltage drop ΔV at the load resistor. Note that this value is independent of the different load resistors chosen in our experiments. Therefrom, we conclude that for this oscillation the sample voltage is one of the relevant dynamical parameters. The current amplitude of this oscillation is given as a function of the voltage via $\Delta I=\Delta V/R_L$. For current values higher than 3 μ A, both frequency and amplitude are lowered to about 1.5 kHz and 50 mV, respectively. Increasing the bias voltage further, we find a systematic decrease of the oscillation amplitude, whereas the frequency varies without any notable simple systematics, but remaining in the range of a few kHz. In contrast to the former, this type of oscillation does not behave in a strictly periodic manner. We have observed quasiperiodic, chaotic, and highly turbulent signals.

Taking into account the characteristic shape of the oscillations [Figs. 3(a)–3(d)], we can clearly distinguish between two types of oscillations that behave differently as a function of the mean current (and also as a function of other control parameters, as we will see below). Note that these features could be found in a variety of samples, but they could differ in their quantitative values from sample to sample, even from setup to setup. In the following, we will talk about *circuit-limited oscillations* (CLO's) in the case of the high-amplitude oscillations at lower dc currents (type I), and about *structure-limited oscillations* (SLO's) in the case of lower amplitudes at dc currents higher than 3 μA (type II) for the sample discussed above. The following discussion will justify this terminology.

IV. CIRCUIT-LIMITED OSCILLATIONS

We start our model considerations with the simple form of the CLO's which are suggestive of the relaxation process due to the charging and discharging of a capacitance. Moreover, the observed proportionality of fre-

quency f and dc current I_{dc} can be written as

$$I_{dc}=Qf \ , \tag{1}$$

where the proportionality constant Q has the units of a charge. This means that in every cycle of the oscillation a constant amount of charge passes through the sample, though these features of our experimental results can be modeled as follows.

Assuming two conducting states each given by a resistance R_1, R_2 ($R_1 > R_2$), respectively, and a certain voltage range where these two states can coexist given by an upper limit V_t and a lower limit V_h (see Fig. 5). For a given load resistor R_L and a bias voltage V_0, the intersection points of the two ohmic lines and the load line are given as

$$V_i = V_0(R_L/R_i+1)^{-1}, \quad i=1,2 \ . \tag{2}$$

These points mark the stable voltages of the system. Now we assume

$$V_1 > V_t > V_h > V_2 \ . \tag{3}$$

In this case, there exists no fixed point, neither on state 1 nor on state 2. Now the system can be regarded as a switch that changes the resistance from R_1 to R_2 at voltages higher than V_t and vice versa for voltages lower than V_h. The intermediary behavior is dominated by the charging and discharging of the capacitance, as seen in Fig. 3(b). The corresponding time constants for the exponential decays are given by

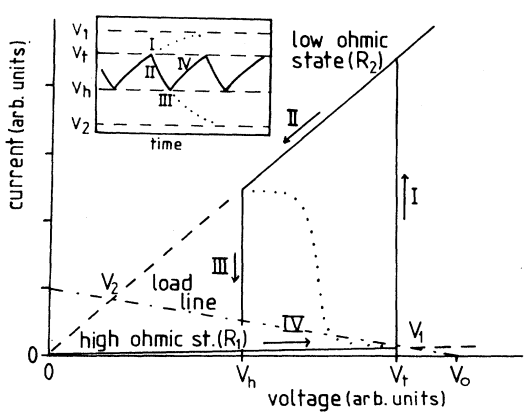

FIG. 5. Model approach to the type-I oscillations (CLO's). The system is regarded as a parallel combination of a capacitance and a switch, the latter being capable to jump from a high ohmic state to a low ohmic state at a certain threshold voltage V_t (step I) and, inversely, from the low ohmic to the high ohmic state at a certain holding voltage V_h ($\ll V_t$) (step III). The intermediary steps (II and IV) are given by the discharge and charge of the capacitance, respectively. For certain bias voltages V_0, there are no intersection points V_1, V_2 of the load line [given by $I(V)=(V_0-V)/R_L$] with the ohmic lines inside the range of stability. Hence, only the dynamical behavior (the resulting time signal is shown in the inset) determines the dc I-V characteristic (dotted curve). Further details are given in the text.

$$\tau_i = CR_L(R_L/R_i+1)^{-1}, \quad i=1,2 \ . \tag{4}$$

Let us start a cycle from V_t with the system being in the high ohmic state. If the sample voltage V becomes greater than or equal to V_t, the system changes its resistance from R_1 to R_2 (step I in Fig. 5). Now the capacitance begins to discharge (step II) and the sample voltage relaxes toward the stable fixed point V_2. After a time

$$T_2 = \tau_2 \gamma_2 \tag{5}$$

with

$$\gamma_2 = \ln\left[\frac{V_t - V_2}{V_h - V_2}\right] , \tag{6}$$

the voltage V_h is reached where the system switches to the high ohmic state (step III). The subsequent charging of the capacitance (step IV) stops after a time T_1

$$T_1 = \tau_1 \gamma_1 \ , \tag{7}$$

$$\gamma_1 = \ln\left[\frac{V_h - V_1}{V_t - V_1}\right] , \tag{8}$$

when the threshold voltage V_t is reached once more and the cycle starts again. In agreement with the experiments, we neglect the switching times (steps I and III). Via two simple integrations, we can calculate the mean voltage of the sample:

$$V_{dc} = (T_1 \bar{V}_1 + T_2 \bar{V}_2)/(T_1 + T_2) \tag{9}$$

with

$$\bar{V}_{1,2} = V_{1.2} \pm \Delta V/\gamma_{1.2}, \quad \Delta V = V_t - V_h \ . \tag{10}$$

With the relation $I_{dc}=(V_0-V_{dc})/R_L$, one can calculate an ND resistive I-V characteristic as a pure consequence of the dynamical behavior of the system. We do not have to make any further physical assumption except for the values of R_1, R_2, and ΔV in order to fit the experimental data to this theory. Before doing this in the following sections, we simplify expression (9) assuming

$$R_1 \gg R_L \gg R_2 \tag{11}$$

according to our experimental situation.

Therefrom, we get $\tau_1 \approx R_L C$, $\tau_2 \approx R_2 C$, $V_1 \approx V_0$, and $V_2 \approx V_0 R_2/R_L \approx 0$. If we can further neglect T_2 with respect to T_1, we obtain

$$V_{dc} = \bar{V}_1 = V_0 - \Delta V/\gamma \tag{12}$$

with

$$\gamma = \ln\left[\frac{V_h - V_0}{V_t - V_0}\right] \tag{13}$$

and

$$I_{dc} = \frac{\Delta V}{R_L \gamma} \tag{14}$$

$$= \Delta V \tau_1 / R_L T_1 = \Delta V C / T_1 \ . \tag{15}$$

Thus we can rewrite Eq. (1) as

$$I_{dc} = \Delta V C f \ . \tag{16}$$

Another important approach is given by the assumption $T_1/R_1 \ll T_2/R_2$. Then it follows that

$$I_{dc} = T_2 \bar{V}_2 / R_2 (T_1 + T_2) \ . \tag{17}$$

We can give a concrete interpretation of expressions (14)–(17). The charge transport in our system consists mainly of two steps. First, the capacitance is charged over the load resistor, whereas the sample is nearly insulating (step IV in the above description of CLO's). Here the mean current is given by Eq. (14). Second, the capacitance becomes discharged in a shorter time over the low ohmic sample, as described by Eq. (17). The proportionality between the mean current and the frequency is given by Eq. (16), in agreement with our experimental results.

Clearly, the model discussed above is nothing else but a (piecewise) linearized form of the well-known van der Pol oscillator,[14] being generic for spontaneous oscillations occurring for an S-shaped ND resistive device embedded in an outer electrical circuitry. For our semiconductor system having temporal *and* spatial degrees of freedom, we conclude that the first bifurcation from the spatially and temporally homogeneous state is governed by the onset of a cooperative oscillatory state (CLO's) taking advantage of the additional degree of freedom available from an outer capacitance. Further, this effect can be used to learn a lot about the physics of avalanche breakdown, as we will see in the following section.

V. EXPERIMENTAL RESULTS II—CONTROL PARAMETERS

A. Current-voltage characteristic and dynamical behavior

In Sec. IV, we calculated the mean sample voltage and the mean current as a function of the applied bias voltage V_0 in the case of CLO's. We have found that, in the limit given by Eq. (12), the mean sample voltage is a unique function of V_0 and independent of the load resistor R_L. Thus the characteristic $I(V)$ should depend on the load resistor in the way that $I \sim 1/R_L$ holds for a fixed sample voltage. We have tested this prediction using different load resistors ($R_L = 100$ kΩ, 200 kΩ, and 1 MΩ) and found I-V characteristics which are stretched with respect to each other by the inverse of R_L, as displayed in Fig. 6(a). This R_L dependence is no longer valid when the characteristics leave the regime of CLO's, and the voltage becomes a unique function of the current. To fit the experimental results by Eqs. (12) and (14), we must make no further assumptions except using the experimentally obtained values for V_t, V_h, and R_L. Comparison between experimental [Fig. 6(a)] and theoretical [Fig. 6(b)] curves shows good agreement in the range where the characteristic is governed by the (regular) CLO mode. Thus we have demonstrated that in a certain region the I-V characteristic—covering more than two orders of magnitude of the averaged current value—is governed only by the dynamical behavior of the system.

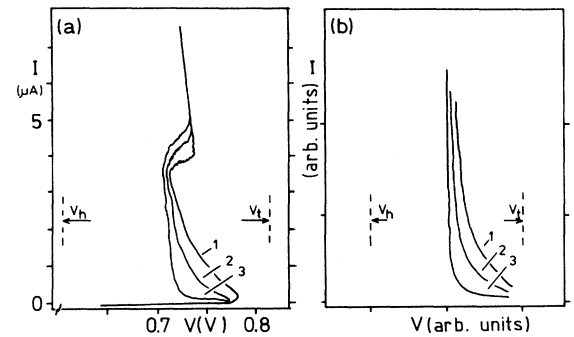

FIG. 6. (a) Current-voltage characteristics measured for different load resistors: (1) 100 kΩ, (2) 200 kΩ, and (3) 1 MΩ (T=4.18 K, B=0 mT). For lower currents, the characteristics are stretched with respect to each other for a given sample voltage according to the inverse ratio of the applied load resistors, whereas in the upper part, the characteristics become identical. (b) Theoretical characteristics (in arbitrary units) obtained from Eq. (14) with three different values for R_L (ratio 1:2:10, according to our experiments).

B. Magnetic field as control parameter

The most important control parameter next to the applied voltage currently used in low-temperature semiconductor experiments is a perpendicular magnetic field. Due to the high mobility of the charge carriers, the system is very sensitive to magnetic fields, even in the range of a few mT.[8] We have again measured the amplitude and frequency for several fixed mean currents in the range of CLO's and SLO's as a function of the applied magnetic field. For the CLO's we found that both amplitude and frequency are independent of the magnetic field in the range of $0 \le B \le 50$ mT. Only the absolute values of V_t and V_h are shifted to higher voltages due to the magnetic field. We emphasize that the mechanism of the CLO's is indispensable to know, in order to determine the exact magnetic-field dependence of the breakdown voltage, as will be reported elsewhere.[19]

On the other hand, the SLO's are very sensitive to the influence of the magnetic field. The amplitude as well as the frequency of these oscillations can be changed drastically by magnetic fields even in the range of 10^{-4} T. For magnetic fields higher than 5 mT, we have noted a shift toward higher frequencies and lower amplitudes, as can be seen in Fig. 7 for a typical sample. In the range of SLO's, different bifurcation phenomena, such as quasiperiodicity, chaos, and rising noise (connected to higher magnetic fields), could also be observed, as was reported in detail elsewhere.[8]

C. Outer capacitance as a control parameter

An obvious possibility to test the predictions of our theory of CLO's is to add an outer capacitance to the setup and to check its influence on the oscillatory behavior. As can be seen from Eq. (16), the effective capacitance of the setup itself can be calculated by the slope of the relation between frequency and current divided by the volt-

age amplitude of the spontaneous oscillations. In this way, we obtain a capacitance C_0 of about 400 pF. By now adding artificially higher capacitances C_a, we have checked that all the above features of the CLO's, especially the independence of the amplitude and the linear increase of the frequency both as a function of the mean current, also hold for the higher capacitances. Again plotting amplitude and frequency for a fixed bias voltage (resulting in a fixed current) as a function of $C=C_0+C_a$ (Fig. 8), we find that in the case of SLO's the frequency is not affected by capacitances smaller than some nF. Only for larger values, does the low-pass filtering effect of the capacitance in combination with the sample resistance become important. The amplitude of the SLO's becomes suppressed and new oscillatory states appear in a lower-frequency range, resulting in a broadband noise for capacitances of more than 10 nF (see Fig. 8). On the other hand, the frequency of the CLO's decreases continuously with increasing outer capacitance C. However, this decrease is not inversely proportional to the capacitance, as could be suggested by a cursory look at Eq. (16). Looking at the amplitude behavior of the CLO's, we note that the amplitude decreases with increasing capacitance. Taking into account this effect, we see that these results also agree with the theory of CLO's. Equation (16) shows that the product of frequency f and amplitude ΔV has to be inversely proportional to the capacitance for a fixed value of the average current, in agreement with our experimental data, as can be seen from the upper part of Fig. 8.

The decrease of ΔV with increasing capacitance, i.e., increasing time constant, demonstrates the importance of the phenomenon of CLO's as a self-organized pulse experiment measuring, e.g., the generation time of a current filament. In fact, we have neglected this time in our calculations and, nevertheless, have obtained reasonable results. Therefore, we conclude that a current filament can be generated, and annihilated, in times much shorter than the time constants of the CLO's. However, taking into account the decrease of the oscillation amplitude ΔV with increasing time constant, it appears that these short generation and annihilation times can be a result of the overshooting of the sample voltage at the turning points V_t and V_h, respectively. We assume that the "natural" time constants of the filamentation process are reached when ΔV saturates as a function of the outer capacitance C. This effect takes place at frequencies of several hertz. So far, these results agree well with the time constants found in real pulse experiments in the same material, as reported earlier.[20]

Additional information, which can be obtained from

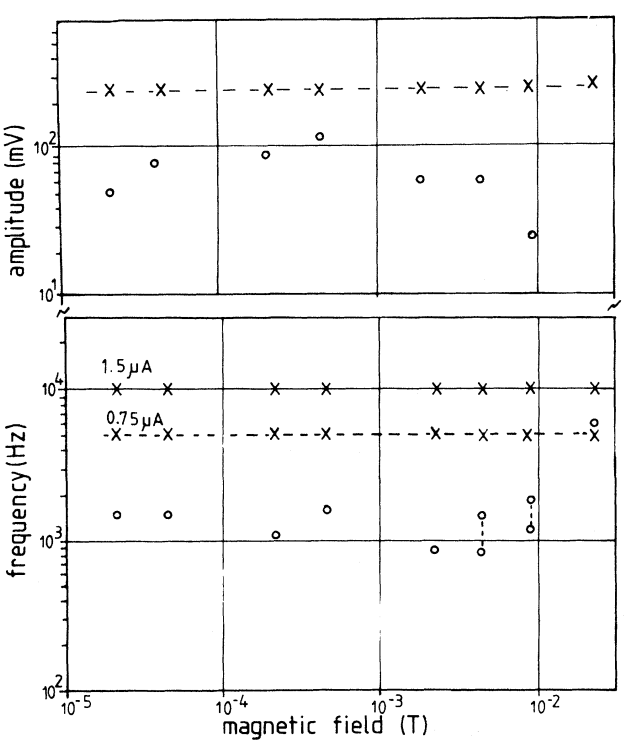

FIG. 7. Oscillatory behavior (amplitude and frequency) as a function of the applied perpendicular magnetic field for the two types of oscillations (CLO's, indicated by crosses, and SLO's, indicated by circles) for fixed values of the dc current (0.75 and 1.5 μA, CLO's, and 5 μA, SLO's). The amplitudes of the two CLO's at the top coincide ($T=4.18$ K, $R_L=100$ kΩ).

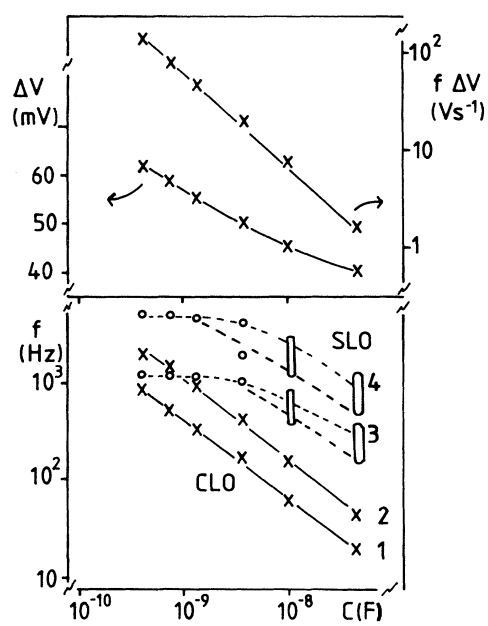

FIG. 8. Log-log plot of oscillatory behavior as a function of the outer capacitance for both types of oscillations. The CLO's are indicated by crosses connected by solid lines, the SLO's by circles connected by dashed lines. The measurements were taken from a distinct sample having a contact distance of 2 mm and a breakdown voltage of about 0.44 V. The frequency behavior is shown in the lower part for four fixed values of the dc current (1) 0.035, (2) 0.115, (3) 1.96, and (4) 2.64 μA. In the upper part, the amplitude ΔV and the product $f\Delta V$ of the CLO's ($I_{dc}=0.115$ μA) are shown as a function of the effective capacitance, applied to the circuit. The slope of the latter curve is -1. The parameters of this measurement were $T=4.18$ K, $B=0$ mT, and $R_L=1$ MΩ.

these experiments, is given by the ratio between the rise time T_2 and the total rotation time of the cycle. From Eq. (17), the latter yields the effective current flow through the sample in the conducting part of the oscillatory cycle:

$$I_2 \approx I_{dc}(T_1+T_2)/T_2 \ . \tag{18}$$

From a time series recorded with high temporal resolution, but without artificially increased outer capacitance (not shown here), this current, flowing during the low-resistive period, can be determined to about 30 μA. This value, if compared with spatially resolved measurements of stationary filaments,[21] would correspond to the size of a current filament of less than 50 μm. From this, it is clear that the CLO's are the result of the firing of a filament and not the result of the breakdown of the whole sample during a short period of time.

VI. STRUCTURE-LIMITED OSCILLATIONS

Let us now briefly discuss our experimental results concerning the second type of oscillations (SLO's). Clearly, the underlying mechanism is not as easily understood as in the case of CLO's. Therefore, we discuss the behavior of the SLO's in a phenomenological way, and we concentrate on the points where clear differences to the behavior of CLO's occur.

The first point concerns the amplitude of these oscillations. Whereas in the case of CLO's high amplitude indicates that the average current is the sole product of the switching of a current filament, in the case of SLO's a dc current is always present and the oscillation is only superimposed on it. This fact gives rise to the assumption that in the parameter regime of SLO's a current filament is already present which is not yet stable in time, and the voltage oscillation is due to the spatiotemporal dynamics of this filament. Moreover, with increasing current, the amplitude of the oscillation decreases continuously and becomes zero when the I-V characteristics enter their positive differential resistance branch. Here the formation of a stable current filament occurs.[5,21] On the other hand, it has been shown theoretically that, with decreasing current, at a certain critical current value, a stable current filament can undergo a Hopf bifurcation, resulting in a breathing mode of the filamentary state.[22] This means that an oscillation bifurcates from the temporally stable state starting from zero amplitude at finite frequency. So far, this theory agrees well with our experimental results. This provides a further hint that the oscillatory mechanism of the SLO's is closely connected to the spatial structure formation.

The typical frequency range of the SLO's is in the order of several kilohertz (see Fig. 4), consequently being much slower than the possible time constant of the generation mechanism of a current filament occurring during an oscillatory cycle of the CLO's. Moreover, the frequency is not affected by a slight variation of the outer capacitance, as can be seen from Fig. 8. Thus an oscillation mechanism involving the global quantity of the external voltage as a dynamical variable seems to be unlikely, and other order parameters must be considered to govern the time constant of such an oscillatory cycle. An additional feature of SLO's is the apparently more complex dynamical structure [see Fig. 3(d)], which cannot be the result of a dynamics involving only two degrees of freedom, as in the case of CLO's. Considering the spatial character of this oscillation, it can be understood that the dynamics of SLO's might be the result of different competing spatial modes based on a local oscillation mechanism, such as the dielectric relaxation or energy relaxation mechanisms.[4] Also, the strong influence of the perpendicular magnetic field (Fig. 7) on the SLO's can be understood to be the result of the interaction between the magnetic field and the filamentary structure, being localized at the phase boundary between the high and the low conducting states. As a symmetry-breaking agent, the perpendicular magnetic field acts in a different way on each of the two filament borders, as has been shown in experiments with n-type GaAs,[23] and p-type Ge.[24] Moreover, it has been reported earlier that a magnetic field perpendicular to the current flow acts in a different way on this type of oscillation.[8] Thus the magnetic-field dependence in our experiments also underlines the spatial character of the second type of oscillation, therefore named the SLO.

VII. CONCLUSION

We have presented a systematic overview on the oscillatory behavior of the system of p-type Ge at the onset of avalanche breakdown as a function of a variety of control parameters. We have found that there is evidence for two different oscillatory modes, which apparently can be distinguished according to their spatial character. As a consequence, we have proposed a classification of the oscillations into structure-limited and circuit-limited oscillations. Especially the latter could be described in a qualitatively and quantitatively satisfying way by a simple linearized switching model. The importance of this classification is given by two points of view.

First, we have found a bifurcation scheme for a system displaying S-shaped negative differential resistance. Starting from the high ohmic homogeneous state, the system enters an oscillatory state which can be described by the mechanism of circuit-limited oscillations. It is reflected by a negative differential current-voltage characteristic, which depends on the load resistor and can be calculated exactly by our theory. With a further increase of current, the structure-limited oscillations appear as a new type, before the system enters a positive differential resistance branch of the characteristic connected to the formation of a stable current filament. The two oscillatory modes are sketched in Fig. 9 according to our proposi-

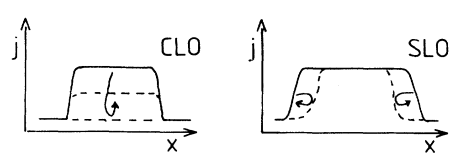

FIG. 9. A sketch of the two possible oscillatory modes displaying the current density as a function of the transverse spatial coordinate. On the left side, firing mode (CLO's); on the right side, breathing mode (SLO's) of a current filament.

tions.

Second, our model of circuit-limited oscillations has important physical consequences. Using this model, we can reduce the physics of the system to a couple of relevant parameters, which can be measured easily by evaluating the oscillatory behavior. For this, we have given some examples and found an interesting insight into the physics of avalanche breakdown.

Finally, we emphasize that there is no reason why the general features described in this paper should be limited to the system of p-type Ge. Experimental results, which can be interpreted in equal terms, have already been reported for the system of n-type GaAs (Refs. 13 and 17) and also for the nonelectrical transport system of avalanches in the flow of a sandpile.[25] Thus we assume that equal or similar results can be obtained for a large variety of systems displaying current controlled negative differential resistance or analogous transport behavior.

ACKNOWLEDGMENTS

The authors would like to thank K. Aoki, U. Buschmann, H. M. Jaeger, and E. Schöll for valuable discussions. This work was supported by a grant of the Deutsche Forschungsgemeinschaft.

[1]B. K. Ridley, Proc. Phys. Soc. **82**, 954 (1963).

[2]J. Peinke, D. B. Schmid, B. Röhricht, and J. Parisi, Z. Phys. B **66**, 65 (1987).

[3]U. Rau, J. Peinke, J. Parisi, and R. P. Huebener, Z. Phys. B **71**, 305 (1988).

[4]E. Schöll, *Nonequilibrium Phase Transitions in Semiconductors* (Springer, Berlin, 1987).

[5]K. M. Mayer, R. Gross, J. Parisi, J. Peinke, and R. P. Huebener, Solid State Commun. **63**, 55 (1987); K. M. Mayer, J. Parisi, and R. P. Huebener, Z. Phys. B **71**, 171 (1988).

[6]D. Jäger, H. Baumann, and R. Symanczyk, Phys. Lett. A **117**, 141 (1986); H. Baumann, R. Symanczyk, C. Radehaus, H.-G. Purwins, and D. Jäger, *ibid.* **123**, 421 (1987).

[7]C. Radehaus, T. Dirksmeyer, H. Willebrand, and H.-G. Purwins, Phys. Lett. A **125**, 92 (1987); H.-G. Purwins, G. Klempt, and J. Berkemeier, in *Festkörperprobleme,* Vol. 27 of *Advances in Solid State Physics,* edited by P. Grosse (Vieweg, Braunschweig, 1987), p. 27; H.-G. Purwins, C. Radehaus, and J. Berkemeier, Z. Naturforsch. **43a**, 17 (1988).

[8]J. Peinke, A. Mühlbach, R. P. Huebener, and J. Parisi, Phys. Lett. **108A**, 407 (1985); J. Peinke, B. Röhricht, A. Mühlbach, J. Parisi, Ch. Nöldeke, R. P. Huebener, and O. E. Rössler, Z. Naturforsch. **40a**, 562 (1985); J. Peinke, J. Parisi, A. Mühlbach, and R. P. Huebener, *ibid.* **42**, 441 (1987); J. Peinke, J. Parisi, B. Röhricht, B. Wessely, and K. M. Mayer, *ibid.* **42**, 841 (1987); U. Rau, J. Peinke, J. Parisi, R. P. Huebener, and E. Schöll, Phys. Lett. A **124**, 335 (1987); R. P. Huebener, J. Peinke, and J. Parisi, Appl. Phys. A **48**, 107 (1989), and references therein.

[9]S. W. Teitsworth, R. M. Westervelt, and E. E. Haller, Phys. Rev. Lett. **51**, 825 (1983); S. W. Teitsworth and R. M. Westervelt, *ibid.* **56**, 516 (1986); E. G. Gwinn and R. M. Westervelt. *ibid.* **57**, 1060 (1986); **59**, 157 (1987); S. W. Teitsworth, Appl. Phys. A **48**, 127 (1989), and references therein.

[10]G. A. Held, C. Jeffries, and E. E. Haller, Phys. Rev. Lett. **52**, 1037 (1984); G. A. Held and C. Jeffries, *ibid.* **55**, 887 (1985); **56**, 1183 (1986).

[11]K. Aoki, T. Kobayashi, and K. Yamamoto, J. Phys. (Paris) Colloq. **42**, C7-51 (1981); J. Phys. Soc. Jpn. **51**, 2373 (1982); K. Aoki and K. Yamamoto, Phys. Lett. **98A**, 72 (1983); K. Aoki, O. Ikezawa, N. Mugibayashi, and K. Yamamoto, Physica B **134**, 288 (1985); K. Aoki and K. Yamamoto, Appl. Phys. A **48**, 111 (1989), and references therein.

[12]S. B. Bumeliene, J. Pozhela, K. A. Pyragas, and A. V. Tamasevicius, Physica B **134**, 293 (1985); S. B. Bumeliene, J. Pozhela, and A. V. Tamasevicius, Phys. Status Solidi B **134**, K71 (1986); K. A. Pyragas, J. Pozhela, A. V. Tamasevicius, and J. Ulbikas, Fiz. Tekhn. Poluprovodn. **21**, 545 (1987) [Sov. Phys.—Semicond. **21**, 335 (1987)]; J. Pozhela, A. V. Tamasevicius, and J. Ulbikas, Solid State Electron. **31**, 805 (1988); J. Pozhela, Z. N. Tamaseviciene, A. V. Tamasevicius, J. Ulbikas, and G. V. Bandurkina, Phys. Status Solidi A **110**, 555 (1988); J. Pozhela, A. Namajunas, A. V. Tamasevicius, and J. Ulbikas, Appl. Phys. A **48**, 181 (1989), and references therein.

[13]A. Brandl, T. Geisel, and W. Prettl, Europhys. Lett. **3**, 401 (1987); U. Frank, A. Brandl, and W. Prettl, Solid State Commun. **69**, 891 (1989); J. Spangler, A. Brandl, and W. Prettl, Appl. Phys. A **48**, 143 (1989), and references therein.

[14]B. Van der Pol, Philos. Mag. **3**, 65 (1927); J. J. Stoker, *Nonlinear Vibrations* (Wiley, New York, 1950); N. Minorsky, *Nonlinear Oscillations* (Van Nostrand, Princeton, 1962); M. P. Shaw and I. J. Gastman, Appl. Phys. Lett. **19**, 243 (1971); M. P. Shaw, H. L. Grubin, and I. J. Gastman, IEEE Trans. Electron Devices **20**, 169 (1973); J. Guckenheimer and P. Holmes, *Nonlinear Oscillations, Dynamical Systems, and Bifurcations of Vector Fields* (Springer, Berlin, 1983).

[15]J. Parisi, U. Rau, J. Peinke, and K. M. Mayer, Z. Phys. B **72**, 225 (1988).

[16]M. Lehr, R. P. Huebener, U. Rau, J. Parisi, W. Clauss, J. Peinke, and B. Röhricht, Phys. Rev. B (to be published).

[17]U. Rau, K. M. Mayer, J. Parisi, J. Peinke, W. Clauss, and R. P. Huebener, Solid State Electron. **32**, 1365 (1989).

[18]U. Rau, Ph.D. thesis, University of Tübingen, 1990.

[19]W. Clauss, U. Rau, J. Parisi, J. Peinke, R. P. Huebener, H. Leier, and A. Forchel, J. Appl. Phys. **67**, 2980 (1990).

[20]J. Peinke, J. Parisi, U. Rau, W. Clauss, and M. Weise, Z. Naturforsch. **44a**, 629 (1989).

[21]K. M. Mayer, J. Peinke, B. Röhricht, J. Parisi, and R. P. Huebener, Phys. Scr. **T19**, 505 (1987).

[22]E. Schöll, Solid State Electron. **32**, 1129 (1989).

[23]A. Brandl, M. Völcker, and W. Prettl, Appl. Phys. Lett. **55**, 238 (1989).

[24]W. Clauss, Ph.D. thesis, University of Tübingen, 1990.

[25]H. M. Jaeger, Chu-heng Liu, and S. R. Nagel, Phys. Rev. Lett. **62**, 40 (1989).